Investigating the Trade-offs Involved in Augmenting a DC Brushless Motor with an Active Heat Sink in Order to Improve Performance.

by

Deron Adriel Browne

Submitted to the
Department of Mechanical Engineering
in Partial Fulfillment of the Requirements for the Degree of

Bachelor of Science in Mechanical Engineering

at the

Massachusetts Institute of Technology

June 2016

Signature of Author: Signature redacted
Department of Mechanical Engineering
May 6, 2016

Certified by: Signature redacted
Hugh M. Herr
Associate Professor, Media Arts and Sciences
Thesis Supervisor

Accepted by: Signature redacted
Anette Hosoi
Professor of Mechanical Engineering
Undergraduate Officer

Investigating the Trade-offs Involved in Augmenting a DC Brushless Motor with an Active Heat Sink in Order to Improve Performance.

by

Deron Adriel Browne

Submitted to the Department of Mechanical Engineering
on May 6, 2016 in Partial Fulfillment of the
Requirements for the Degree of

Bachelor of Science in Mechanical Engineering

ABSTRACT

This thesis seeks to establish solutions to the issue of electric motor heating and the problems it presents for use of these motors in biomechatronic applications. As electric motors are used, their windings heat up and the resulting temperature limits torque. Larger motors may be used to obtain more torque, but this adds undesirable weight to the devices in which they are used. Cooling methods also exist, but do not necessarily consider suitability to bionic applications. This thesis therefore aims to improve the torque output of a given motor by effectively removing heat while minimizing the addition of mass.

I hypothesize that the torque density of an EC-4 pole 30 48V Maxon DC brushless motor can be improved by augmenting it with an electronics fan and an annulus. Results showed that the housing to ambient thermal resistance of the motor was decreased by 68% from the experimentally found value of $11.5KW^{-1}$ to a value of $4.03KW^{-3}$ by using a $4.72 \times 10^{-3}m^3s^{-1}$ ($10\ cfm$ rated) electronics fan. The projected torque density of the motor was also found to be maximally improved from $0.382Nmkg^{-1}$ to $0.393Nmkg^{-1}$.

These results were obtained under the assumptions that the motor could be reasonably represented by its brushed counterpart and that parallel plate fluid dynamics closely approximates annular fluid dynamics. While more investigation is necessary to fully validate the results, they do show that there is potential for using simple methods to significantly improve the torque density of small electric motors. It is possible then that added mass can work to noticeably improve motor performance. There is therefore scope to improve the use of these motors in biomechatronic devices. Smaller, more efficient motors will decrease the weight of these devices and improve their overall efficiency. Bionic devices will thus be one step closer to better mimicking human capability.

Thesis Supervisor: Hugh M. Herr
Title: Associate Professor, Media Arts and Sciences

Contents

Acknowledgements

I would like to thank Molly Schneider and the MISTI office for creating the opportunity for me to connect with the Biomechatronics Lab at the Media Lab. I would also like to thank Brandy Baker and the MIT Mechanical Engineering Undergraduate office for helping to facilitate my thesis. Without you, I would not have had the opportunity to do this thesis.

I would further like to sincerely thank Dr. Luke Mooney and Dr. Kenneth Pasch for their commitment to seeing me through this process. Your patience and willingness to be hands on is greatly appreciated. I would also like to extend my thanks to Laura Gilson for freely rendering assistance during the modeling stage of this thesis. My greatest appreciations to Professor Hugh Herr as well for being my advisor and for allowing me to do my thesis in your lab.

Lastly, I would like to take the opportunity to recognize my family and friends who provided encouragement throughout this process. Your support was a large part of my success in this project.

Chapter 1 - Introduction

DC brushless motors employed in series elastic actuators are the preferred method of torque supply for bio-mechatronic applications[1]. These actuators must produce large[2] torques and large amounts of mechanical power (>100W)[2] in order to adequately replicate or augment torques generated by human muscles. For instance, lower limb joints require torques in excess of 100Nm to meet peak demands for walking in a 100kg individual[2]. These torques and powers must also be applied at relatively low speeds for typical joint activity. Actuators used to replicate human motion should thus be able to replicate this activity.

Unfortunately, rotary electric motors are most efficient at high speeds and low torques since higher torques require higher input currents which in turn drive up winding temperature as they dissipate heat. This heat, if not removed, increases the temperature of all motor components. At a particular temperature, the lamination of the windings breaks down and shorting occurs resulting in motor burnout[3]. Further, the magnetic field strength of the magnets decreases with increasing temperature. These effects both work to decrease the continuous torque that a motor can safely output.

This low torque, high speed operation is the opposite of what is required for replicating human ability. As such, larger motors may be used to obtain a better match or smaller motors may be used with transmission. However, both these solutions add mass and/or inefficiencies. It is therefore necessary to attempt to improve the performance of smaller motors. These smaller more powerful motors are both low in weight and reduce the necessary transmission ratio, thereby reducing complexity and inefficiencies. Heat removal methods may be implemented to achieve this improvement, but the torque density must be maximized. That is to say that any weight added to the motor in efforts to increase efficiency must work to improve the specific torque of the entire actuator setup. There is therefore a tradeoff as all mass added must be viewed in light of the improvement it provides. This thesis aims to examine this tradeoff.

Exoskeletons and robotic prostheses are worn on the body. Increasing the weight of such devices by using larger motors or bulky components for heat removal is undesirable since the user will need to expend increased amounts of metabolic energy to move the device. In addition, heavier devices mean that the power sources used will have to be of an increased electrical capacity. This often means increased mass. It is therefore necessary to minimize the weight of such devices without compromising motor performance.

There are two general ways to improve motor performance. One may attempt to increase motor efficiency by lowering the resistance of the windings (by changing the winding material for instance) or by increasing the motor torque constant. Alternatively, one may choose to more effectively remove heat from the motor, which, as an added benefit, also increases motor efficiency by keeping the windings and magnets cooler. The latter approach has a greater effect and is also more practical. However, this approach does add mass to the motor, but it is possible that the mass added to the motor can act to compensate for the added mass by enabling the motor to produce more torque per unit mass.

In an effort to minimize added mass, a simple fan and a 3D printed annulus were added to the motor. See Figure 1. Fans used to cool electronics are lightweight and seem to work well in their applications. However, the airflow they produce will likely need to be contained. An annulus was thus thought to be necessary. The annulus was 3D printed with ABS plastic since the 3D printing process can produce parts that are light (compared to making the annulus out of metal for instance). If the margin of improvement is significant, there is most definitely potential for better results with more complex solutions. As such I hope that by beginning with a simple solution I can set the baseline for performance improvement.

Improving the torque limit of motors used in biomechanical devices will have a direct impact on the performance of the devices. It is the goal of such devices to mimic human capabilities so that their

operation can seamlessly be coupled to that of the human body. Increasing the torque derived from the DC brushless motors used is a step toward these devices more closely reproducing human ability.

In this thesis, an EC-4 pole 48V Maxon DC brushless motor will be augmented with a fan and annuli and the performance of the motor with and without cooling will be investigated. I aim to quantitatively represent how motor performance is improved and use this representation to concretely demonstrate that this augmentation satisfactorily improves motor performance by increasing the torque density. This will show that simple solutions can significantly improve performance, thereby setting the stage for more refined solutions.

I hypothesize that the torque density of an EC-4 pole 30 48V Maxon DC brushless motor can be improved by augmenting it with an electronics fan and an annulus. See Figure 1. I propose that this will be a more desirable solution than simply using a larger motor as it minimizes added mass.

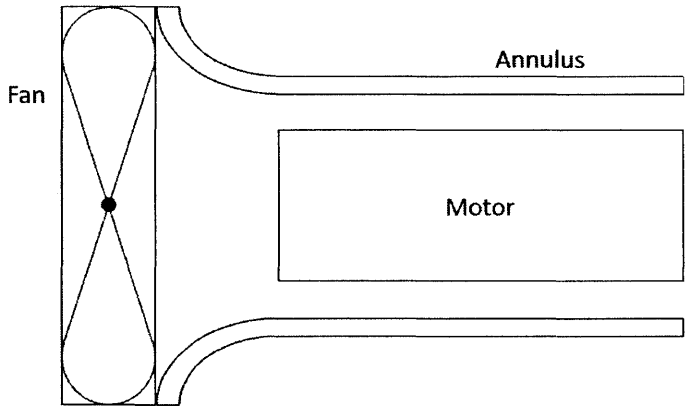

Fig. 1: Diagram showing fan-annulus-motor configuration

Firstly, background on the source of the problem being addressed will be presented. Subsequently, mathematical modeling and results to verify the model will be presented. Results will then be analyzed and discussed in order to provide a conclusive observation.

Chapter 2 - Background

2.1 Limitations of Current Motors

Motors have a maximum allowable torque that they can produce. Running a current, I, through a wire produces heat due to wire resistance, R. This heat accounts for most of the discrepancy between input electrical power, P_{in}, and output mechanical power, P_{mech}, as Fig. 2 illustrates. This power loss, which will be called P_{diss} in reality comes from a few factors: changing conductor resistance, core losses and in overcoming friction. Maxon motors do not use iron cores[3], so there is no loss due to the presence of a core. However, the outer housing of the motor is likely made of a ferrous material. The stationary housing thus sees a changing magnetic flux as the magnets rotate with the rotor. It therefore also experiences associated losses. Nevertheless, these losses along with frictional losses are assumed to be negligible relative to changing winding resistance. Hence, all dissipated power is attributed to winding resistance and is given by equation (1). Note that in my equations, I am approximating the motor as a brushed motor in order to simplify modeling. Commutation is not considered and the resistance, R, used here is simply the combined electrical resistance of two phases of the three phase wye winding configuration. The motor is therefore in one state of block commutation. This simplification can be used since in block commutation, only two phases of the windings are active at any time.

$$P_{diss} = I^2 R \qquad (1)$$

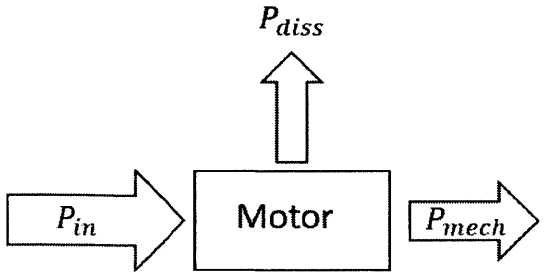

Fig 2 - Flow chart showing power consumption

Some of the power provided to the motor is dissipated as heat. There is thus a limit to how much mechanical power one can extract from a motor. This power loss is also affected by winding resistance, which is itself affected by operating temperature, T, in accordance with the equation below [4, 5, 6].

$$R = R_{ref}[1 + \alpha(T - T_{ref})] \quad (2)$$

In equation (2), R_{ref} represents the winding resistance at a reference temperature, T_{ref}, while α represents the temperature coefficient of resistance of the windings. I assume that the windings are made of pure copper such that $\alpha = 0.0039°C^{-1}$ (i.e. for every degree increase in temperature, the ratio of R to R_{ref} increases by (0.0039). Therefore, the higher the operating temperature, the less efficient the motor is. That is to say that with increasing operating temperature, a diminishing percentage of the electrical power input is able to be used for mechanical power. It is therefore prudent to keep this temperature at a minimum. This can be achieved via a variety of methods for the generic electric motor. In addition, the motor has a maximum allowable temperature it can tolerate. If the heat is not effectively removed, the windings can become too hot and motor burnout may occur.

Furthermore, the creation of this heat negatively affects the magnets used in the motors as well as the motor torque constant, K_t. More explicitly speaking, K_t decreases with temperature according to the relationship outlined in equation (2)[4], with K_t and $K_{t,ref}$ taking the place of R and R_{ref} and the reversible temperature coefficient of induction, α_{mag}, taking the place of α. Magnetic strength is directly related to this relationship[4] and therefore also decreases as temperature increases. In fact, should the motor become hot enough to reach a temperature called the Curie temperature, magnetism is lost permanently[7]. As such, existing electrical motors are limited in their efficiency by the operating temperature of the windings and the driving current.

2.2 Current motor availability

As stated in the introduction, for robotic prostheses and exoskeleton applications, DC brushless motors are generally used[1]. These motors are available in a range of sizes and power ratings. However, more powerful motors tend to be larger and heavier. This is undesirable for robotic applications in the domain of bio-mechatronics since motors are housed on board and they add weight, thereby decreasing efficiency. In the Biomechatronics Lab at MIT's Media Lab, the most popular choice of motor is the EC-4 pole 30 48V Maxon DC brushless motor.

2.3 Current ways of cooling motors

Most popularly, motors are generally air cooled. Air cooling methods may take advantage of natural convection by making use of the motor operating in open air. These methods may also make use of fans attached to the motor shaft to increase air turbulence and velocity around the motor thereby improving heat removal[8]. Fins can be added to the motor housing as well to increase the surface area over which cooling can occur. Water or other fluids are also used, though more rarely so and novel applications are always being created. While these methods are generally accepted, it is unclear whether or not the added mass of these solutions is compensated for by improved performance. Given this uncertainty, it is unclear whether these solutions are appropriate for biomechanical applications. This thesis seeks to clarify this uncertainty by investigating one application of forced convection air cooling.

Chapter 3 - Unaltered Operation

3.1 Mathematical Modeling

The motor operating under unaltered conditions was first modeled. Based on data from the motor specification sheet, we anticipate a linearly proportional relationship between output torque, τ, and input current, i. The constant of proportionality, K_t, is known as the motor torque constant and has a value of $27.6mNmA^{-1}$.

$$\tau = K_t i \quad (4)$$

So if the motor is run at the maximum continuous current of $3.68A$, it should produce $0.1Nm$ of torque.

However, K_t, despite its name, is not a constant. It varies with winding temperature, T_w [6].

$$K_t = K_{t,ref}\left[1 + \alpha_{magnet}\left(T_w - T_{ref}\right)\right] \quad (5)$$

As mentioned previously, α_{magnet} is the temperature coefficient for the magnet used in the motor. In the case of the EC-4 pole 48V Maxon DC brushless motor, an NdFeB magnet is used which has a reversible temperature coefficient of $-0.0012°C^{-1}$. $K_{t,ref}$ is the motor torque constant at a reference temperature, $T_{ref} = 293.15K$ where T_{ref} is taken to be the same as the accepted temperature for determining R_{ref}[6].

We also know that resistance also changes with temperature according to equation (2). Hence, to maintain a constant power of 10W as is done in the experiments detailed later on, the input current would have to be changed as the winding resistance changes. Equation (3) thus becomes

$$\tau = K_{t,ref}\left[1 + \alpha_{magnet}\left(T_w - T_{ref}\right)\right]\sqrt{\frac{10}{R_{ref}\left[1 + \alpha\left(T_w - T_{ref}\right)\right]}} \quad (6)$$

We should expect then to see the following trend for given winding temperatures, T_w.

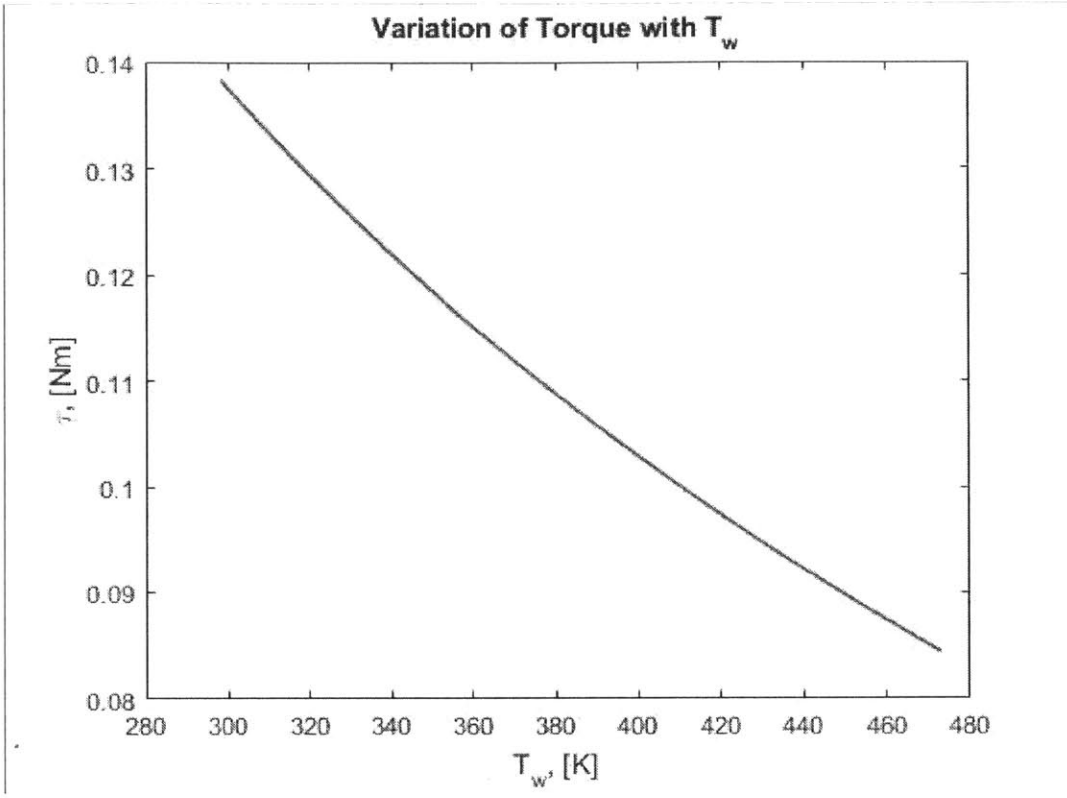

Fig 3: Graph illustrating how winding temperature affects motor torque. Current was altered to maintain a constant power input of $10W$.

3.2 Experimental

In order to test the prediction of motor performance under unaltered conditions, the motor was connected to a power source that consistently outputted $10W$ of power by changing the current and voltage settings as the resistance changed. It was noted, however, that these values deviated minimally from their initial values of $I = 5A$ and $V = 2V$. The winding resistance was calculated over time by using the current and voltage values. The winding temperature was then calculated based on the resistance and the expected torque found based on equation (6).

3.2.1 Hypothesis

Based on prior mathematical modeling, it is expected that the motor torque will lie in the range $0.0844Nm - 0.1383Nm$ as determined by an ambient of $298.15K$ and a maximum allowable winding temperature of $423.15K$. It is also expected that the housing to ambient thermal resistance of the motor will be $7.4KW^{-1}$

3.2.2 Aims

1. Verify the housing to ambient thermal resistance
2. Verify that the steady state temperature of the motor will give a torque that lies in the predicted range.

3.2.3 Apparatus

1. Programmable power supply (used to power motor - see Appendix 1): 9152 30V/18A 540W, B&K Precision, Yorba Linda, CA, USA
2. DC brushless motor: EC-4 pole 48V, Maxon Motors, Sachseln, Switzerland (See Appendix 2)
3. Voltmeter/Ohmmeter (built into power source)
4. Timer
5. Computer to control setup via MATLAB

3.2.4 Experimental Background

3.2.4.1 Mathematical Model

The temperature of the motor windings can be determined by rearranging equation (2).

that is:

$$T_w = \left[\left(\frac{R}{R_{ref}} - 1\right)\frac{1}{\alpha}\right] + T_{ref} \quad (7)$$

R_{ref} can be determined at some T_{ref} and then equation (7) can be used to determine the winding temperature at other resistances. The value of T_w can then be used to find the corresponding torque in accordance with equation (6).

To verify the housing to ambient thermal resistance, we can use a simple thermal circuit as shown in figure 4 below.

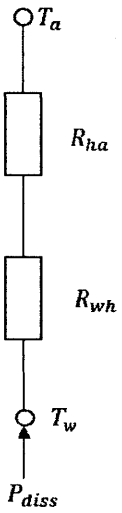

Fig 4: Thermal circuit representation of steady state heat conduction and convection in the motor

This allows us to derive equation (8)

$$P_{diss} = \frac{T_w - T_a}{R_{ha} + R_{wh}} \quad (8)$$

Where ambient temperature is represented by T_a, housing to ambient thermal resistance is represented by R_{ha} and winding to housing thermal resistance is represented by R_{wh}

$$P_{diss} = P_{in} - P_{out} \quad (9)$$

Since the motor is not being commutated, the shaft does not rotate and there is no mechanical power output, $P_{out} = 0$.

$$\Rightarrow P_{diss} = P_{in} = IV \quad (10)$$

Hence, by noting T_a and assuming that the specified $R_{wh} = 0.21KW^{-1}$ (see Appendix 2) is accurate, we can verify R_{ha}.

$$R_{ha} = \left(\frac{T_w - T_\infty}{P_{diss}}\right) - R_{wh} \quad (11)$$

3.2.4.2 Time Constants

A first order dynamic system does not produce a step output in response to a step input. Instead, it gradually approaches its steady state. It is therefore important to consider the time constant for the system. The time constant of a system defines the time required for a parameter in question to increase to 63.2% (or decrease to 36.8%) of its final asymptotic value.

In our situation, there is an exponential response in the resistance to a power step input of $10W$ as the windings heat up. As such, it is necessary to wait a length of time for the system to come to equilibrium. The motor time constant is 1180s (approximately 19 minutes). One would need to wait about an hour for each test to obtain the response shown in figure 5 below.

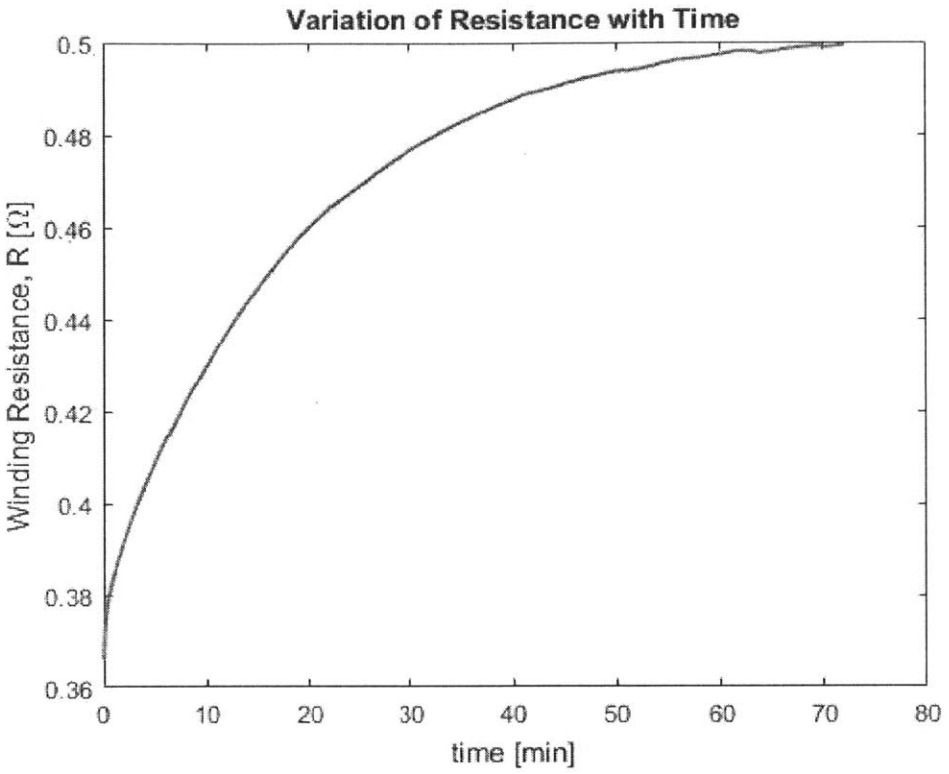

Fig. 5: Graph showing response of winding resistance to a power step input of $10W$.

As an alternative, we chose to allow the setup to run for one time constant, record data, and then use MATLAB to fit a curve to the data in order to predict the steady state of the motor.

3.2.5 Procedure

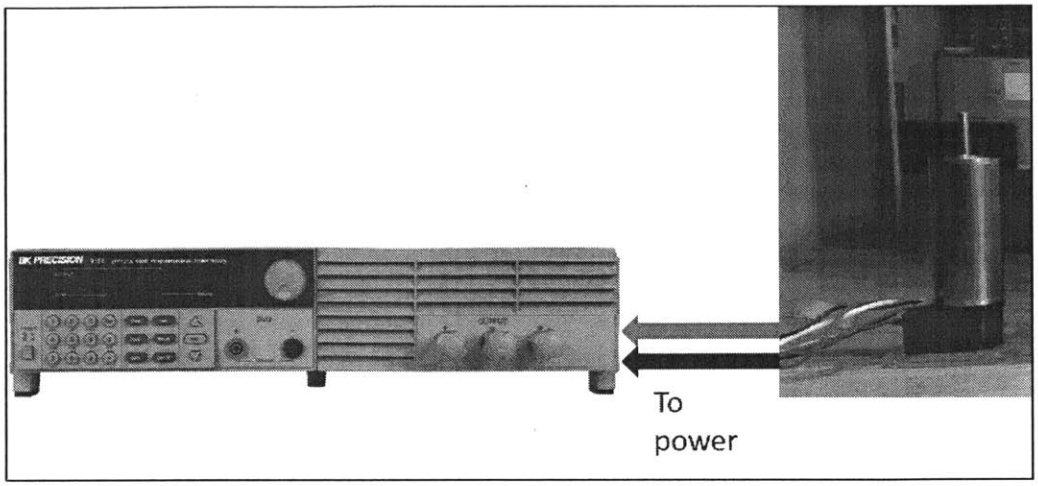

Fig. 6: Diagram showing experimental setup for motor under unfanned operation

1. Set up apparatus as shown in figure 6.
2. Note T_a and record it
3. On the programmable power supply, set I to $5A$ and V to $2.5V$ to create a power output of 10W.
4. At each time step, sample I and V and calculate the corresponding R. Find the winding temperature and alter the input current and voltage to maintain the power input. Do this for one time constant.
5. Plot data and fit a curve to the data to predict the steady state winding resistance.
6. Use the steady state resistance to determine steady state T_w and the projected steady state τ.

3.3 Results

From the unaltered operation, with 10W dissipated, the maximum winding resistance was 0.5Ω.

Hence, according to equation (19).

$$T_w = 413.17K$$

From this, we can find the projected steady state torque via equation (6).

$$\tau = 0.1181\ Nm$$

From the motor specification. sheet, the motor mass is $0.3\ kg$. We can therefore express the torque density as

$$\tau_{dens} = 0.393\ Nmkg^{-1}$$

The housing to ambient thermal resistance was then found using equation (2)

$$R_{ha} = 11.5KW^{-1}$$

Chapter 4 - Fan Only

We will now investigate how adding a fan only affects the temperature of the windings. It was assumed that using a fan only will cause much of the airflow to be dispersed to the environment thereby nullifying the impact of adding a fan. Hence, the full augmentation to the motor included both a fan and an annulus. However, this assumption needed to be tested. The tests were carried out purely experimentally as is outlined below. The fan was placed in cross flow since in reality, if it was to mounted in parallel flow, it would either at one end physically obstruct the rotating shaft of the motor or at the other end act to futilely cool the plastic encasing the motor controller rather than the metal motor housing. In addition, since bionic devices generally need to be compact, the fan was also placed at three different distances from the motor that covered a small overall range, but were disparate enough to see a correlation between proximity of the fan to the motor and the motor's performance.

4.1 Hypothesis

It is hypothesized that using a fan only will improve motor performance, but the improvement will be less than what will be observed with both a fan and an annulus. It is expected that the improvement will diminish with distance from the motor.

4.2 Aims

Measure the new housing to ambient thermal resistance for each of three distances: $5mm, 15mm, 30mm$.

Measure the steady state temperature in each case.

Calculate the total mass added.

Calculate the corresponding torque and specific torque.

4.3 Apparatus

1. Programmable power supply (used to power motor - see Appendix 1): 9152 30V/18A 540W, B&K Precision, Yorba Linda, CA, USA
2. DC brushless motor: EC-4 pole 48V, Maxon Motors, Sachseln, Switzerland (See Appendix 2)
3. Timer
4. DC power supply (used to power fan – see Appendix 3): 6282A, Hewlett Packard, Palo Alto, CA, USA
5. Voltmeter/Ohmmeter (built into power source)
6. 10 cfm rated electronics fan: PSAD14010BH, Aavid Thermalloy, Laconia NH, USA (See Appendix 4)
7. Computer to control setup via MATLAB

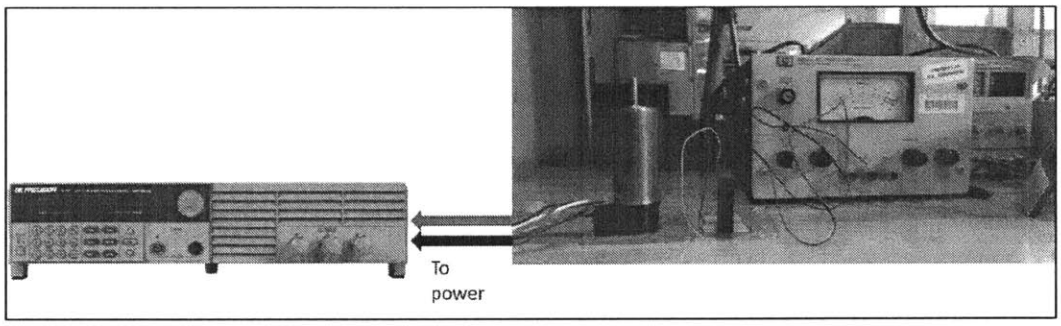

Fig. 7: Diagram showing experimental setup for motor under fanned operation with no annulus.

4.3 Procedure

1. Set up apparatus as shown in figure 7 above.
2. Note T_a and record it
3. Turn on the DC power supply to turn on the fan and position the fan in cross flow, 5mm away from the motor.
4. On the programmable power supply, set I to $5A$ and V to $2.5V$ to create a power output of 10W.

5. At each time step, sample I and V and calculate the corresponding R. Find the winding temperature and alter the input current and voltage to maintain the power input. Do this for one time constant.
6. Plot data and fit a curve to the data to predict the steady state winding resistance.
7. Use the steady state resistance to determine steady state T_w and the projected steady state τ.
8. Increase the distance to 15mm and 30mm, repeating steps 4 through 6 each time.

4.2 Results

After adding a fan of mass 0.0144kg, we obtain the following results.

	5mm	15mm	30mm
Maximum Resistance, R [Ω]	0.4045	0.4068	0.4101
Steady State Winding Temperature, T_w $[K]$	340.3	342.0	344.5
Steady State Torque, τ $[Nm]$	0.1218	0.1212	0.1203
Added Mass, m $[kg]$	0.3144	0.3144	0.3144
Torque Density, τ_{dens} $[Nmkg^{-1}]$	0.3874	0.3855	0.3826
Corresponding R_{ha} $[KW^{-1}]$	4.03	4.20	4.45

Table 1: Table listing measured and calculated parameters for each fan distance.

Chapter 5 - Annular Flow

For annular flow, the fan will now be mounted onto a 3D printed annulus which is itself slid over the motor. This will contain the airflow produced by the fan such that it is maximally directed over the motor. This configuration is pictured in figure 8 below and is also represented by a schematic in figure 1.

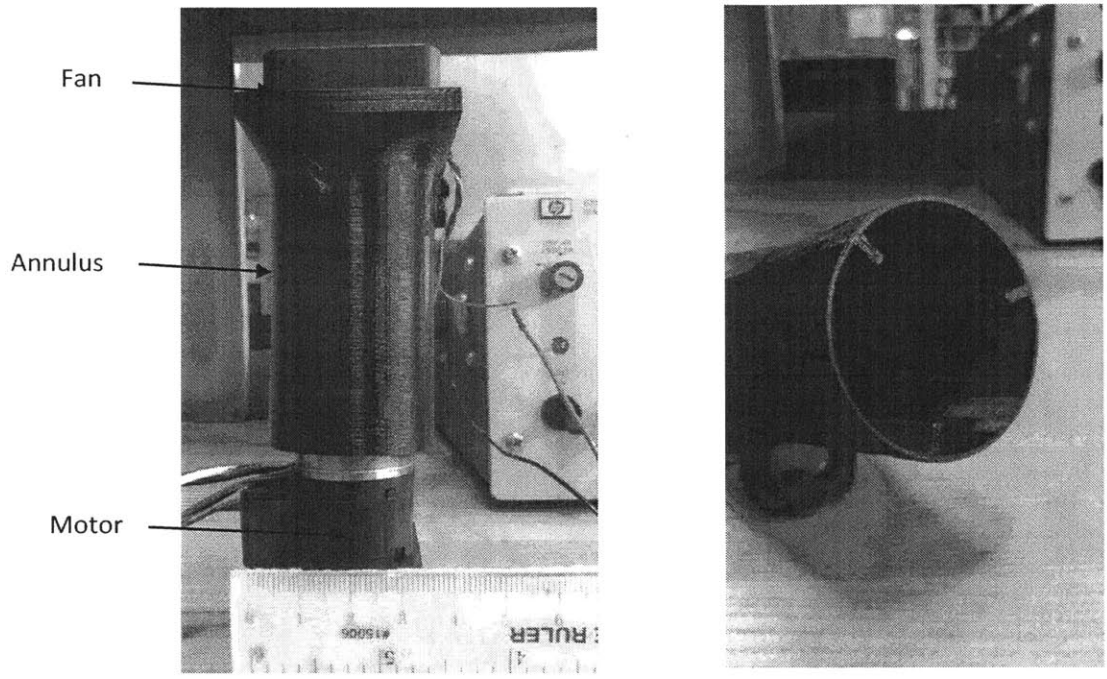

Fig. 8: Pictures showing annulus and how it was installed over the motor. The picture on the right shows the tabs that were used to keep the annulus centered over the motor

5.1 Mathematical Modeling

To find an expression for the temperature of the windings, we first need to determine the temperature of the housing under flow conditions. We have chosen to model the motor housing as a flat plate having heat generated on one side by the windings. The plate will have a length equal to the length of the motor and a width equal to the circumference of the motor housing.

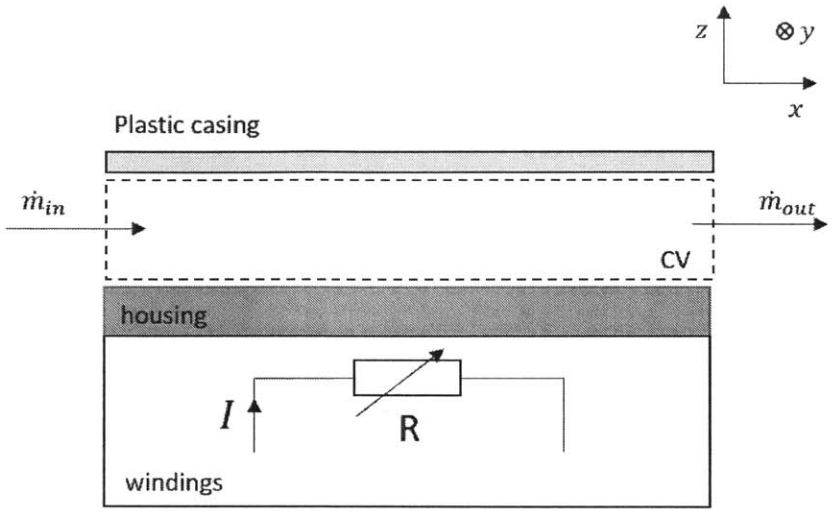

Fig 9: Schematic of parallel plate approximation used to model flow in annulus.

If we consider that there is no conduction in the x direction, we can assume that all heat produced by the windings (represented by the electrical circuit in figure 9 above) is eventually dissipated to the air in the annulus. This occurs via convection and we know that the heat lost per unit surface area, A_{surf}, is given by Newton's law of cooling by convection in equation (7) where q' is the power dissipated per unit surface area, T_h refers to the temperature of the motor housing and h is the thermal coefficient of convection.

$$q' = \frac{P_{diss}}{A_{surf}} = -\frac{I^2 R}{A_{surf}} = h(T_a - T_h) \quad (7)$$

Recall equation (2):

$$R = R_{ref}[1 + \alpha(T_w - T_{ref})]$$

Hence by substituting into (5),

$$-T_h = T_\infty + \frac{I^2 R_{ref} \alpha T_w}{A_{surf} h} + \frac{I^2 R_{ref}[1 - \alpha T_{ref}]}{A_{surf} h} \quad (8)$$

Now, we can represent the temperature of the windings using a simple thermal circuit as shown in Fig 10 below.

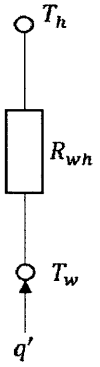

Fig 10: Thermal circuit representation of steady state heat conduction in the motor

We can therefore say that

$$T_w - T_h = q' R_{wh} \quad (9)$$

$$T_w = \frac{I^2 R_{ref}\left[1 - \alpha T_{ref}\right]\left(\frac{1}{A_{surf} h} - R_{wh}\right) + T_\infty}{\left[1 - I^2 R_{ref} \alpha \left(\frac{1}{A_{surf} h} - R_{wh}\right)\right]} \quad (10)$$

We now need to find an expression for h. This was done via Nusselt number correlations for laminar flow equation (11)[9] and turbulent flow equation (12)[10] over an isothermal plate and for $Pr \geq 0.6$.

$$Nu_x = \frac{h_x x}{k} = 0.332 Re_x^{0.5} Pr^{\frac{1}{3}} \quad (11)$$

$$Nu_x = \frac{h_x x}{k} = 0.0.0296 Re_x^{\frac{4}{5}} Pr^{\frac{1}{3}} \quad (12)$$

Where Nu_x is the Nusselt number defined with respect to the distance along the motor, x. Re represents Reynolds number, Pr represents the Prandtl number and k refers to the thermal coefficient of conduction for the motor housing.

If we draw a control volume between the fan and the beginning of the (uniformly shaped) annulus as shown in figure 11 below, we can use the flow rate of air coming off of the fan to obtain that the velocity, u_1 of air coming out of this control volume and thus entering the annular region is given by equation (13).

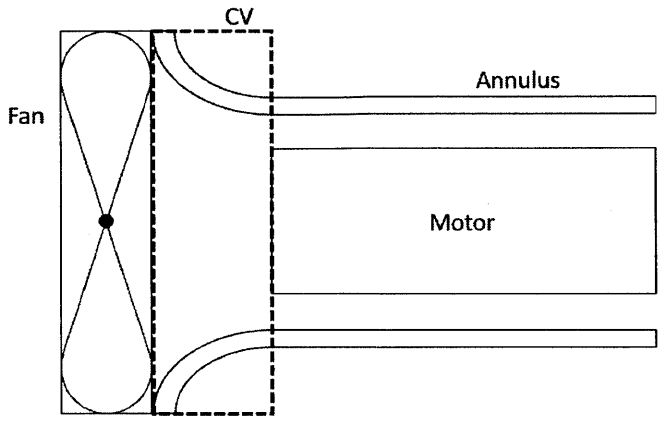

Fig. 11: Schematic showing the control volume being considered in equation (13)

$$u_1 = \frac{\dot{V}_{fan}}{60A_{annulus}} = \frac{\dot{V}_{fan}}{60\pi\left(\frac{r_{mot}^2}{r^{*2}} - r_{mot}^2\right)} \quad (13)$$

Where $\dot{V}_{fan}$ is the rated volumetric air flow rate produced by the fan, $A_{annulus}$ is the cross-sectional area of the annular region, r_{mot} is the cross-sectional radius of the motor and $r^* = \frac{r_{mot}}{r_o}$ with r_o representing the outer radius of the annulus.

We can therefore define the Reynold's number here as

$$Re = \frac{v_1 D_h}{\vartheta} = \frac{v_1}{\vartheta} 2(r_o - r_{mot}) = \frac{\dot{V}_{fan}\left(\frac{r_{mot}}{r^*} - r_{mot}\right)}{30\vartheta\pi\left(\frac{r_{mot}^2}{r^{*2}} - r_{mot}^2\right)} \quad (14)$$

Where D_h is the hydraulic diameter of the annulus.

However, equation (14) only gives a first approximation to the Reynolds number. When fluid is forced through a reduced space, the flow rate changes due to pressure drops. We need to find the actual flow rate.

Figure 8 below presents a schematic of what occurs when fluid is forced over a bank of tubes, parallel to the direction of flow. Just as in the annular situation, the free area is significantly reduced and the dynamics of the flow must compensate for this change. Should we take a cross section of annular flow as in figure 11, we can also see that figure 12 is a close approximation to the configuration being analyzed in this thesis. We can therefore model the annulus according to the following configuration.

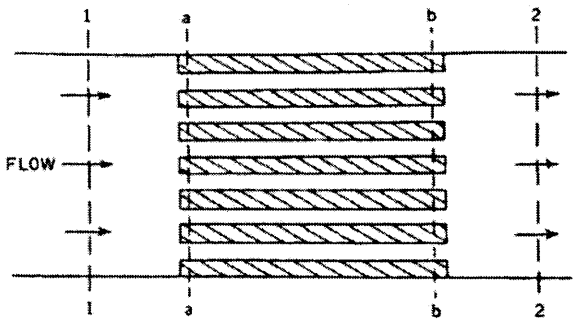

Fig 12: Reproduced from Kays and London[11], Fig 2-10

The pressure drop due to a particular r^* can then be found from equation (15)[11] below that models pressure drop, ΔP, due to flow in the configuration presented in figure 8.

$$\frac{\Delta P}{P_1} = \frac{G^2 v_1}{2 g_c P_1}\left[(K_c + 1 - \sigma^2) + 2\left(\frac{v_2}{v_1} - 1\right) + f\left(\frac{A}{A_c}\right)\left(\frac{v_m}{v_1}\right) - (1 - \sigma^2 - K_e)\left(\frac{v_2}{v_1}\right)\right] \quad (15)$$

G is defined as the flow stream mass velocity and is given by $\frac{W}{A_c}$ where W is the mass flow rate and A_c is the free flow cross-sectional area.

K_c and K_e are the contraction and expansion loss coefficients for flow at the entrance and exit of the configuration of figure 12. They were determined by interpolating from figure 13 below and finding equations for each the graphs.

σ is the ratio of free flow area to total frontal area.

v_1 and v_2 are the specific volumes at the regions shown by the dotted lines 1 and 2 in figure 8. $v_m$is the mean specific volume. Since the fluid being considered is air, $v_1 = v_2 = v_m$.

A is the total heat transfer area.

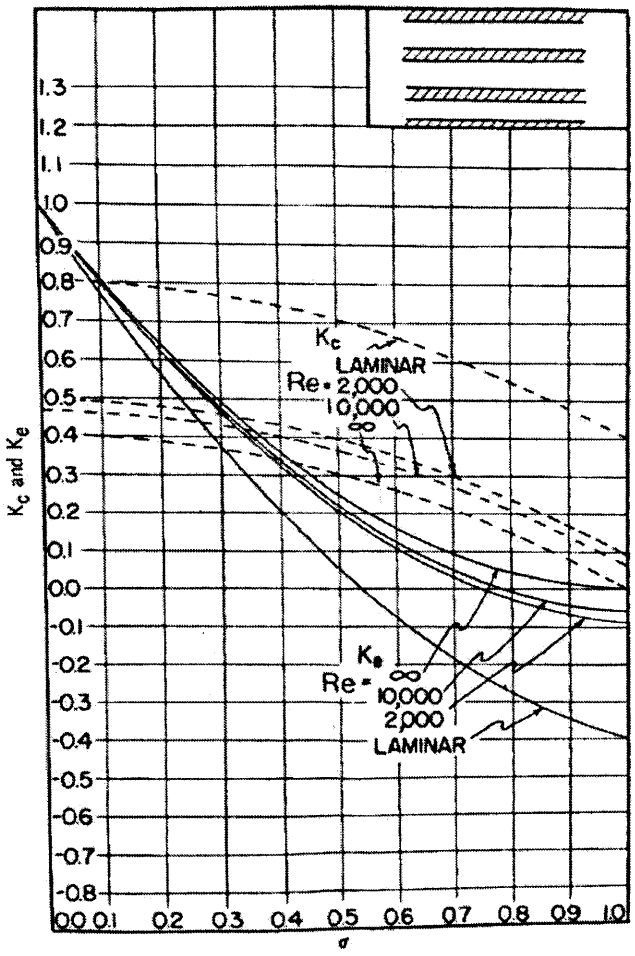

Fig 13: Reproduced from Kays and London Fig 5-3.

Re was found for each r^* being considered using the flow rate as determined by the fan. For $Re \leq 2000$, the $Re = 2000$ graph was used. For $2000 < Re \leq 10000$, the $Re = 10000$ was used. For $Re > 10000$, the $Re = \infty$ graph was used. Subsequently, the correct K values were determined using σ values and the equations obtained from interpolation.

The graphs for ΔP vs r^* were then plotted on the same axes as the fan curve as in figure 14 below and the intersections[12] found. These solutions provide the actual operational flow rates for each r^*.

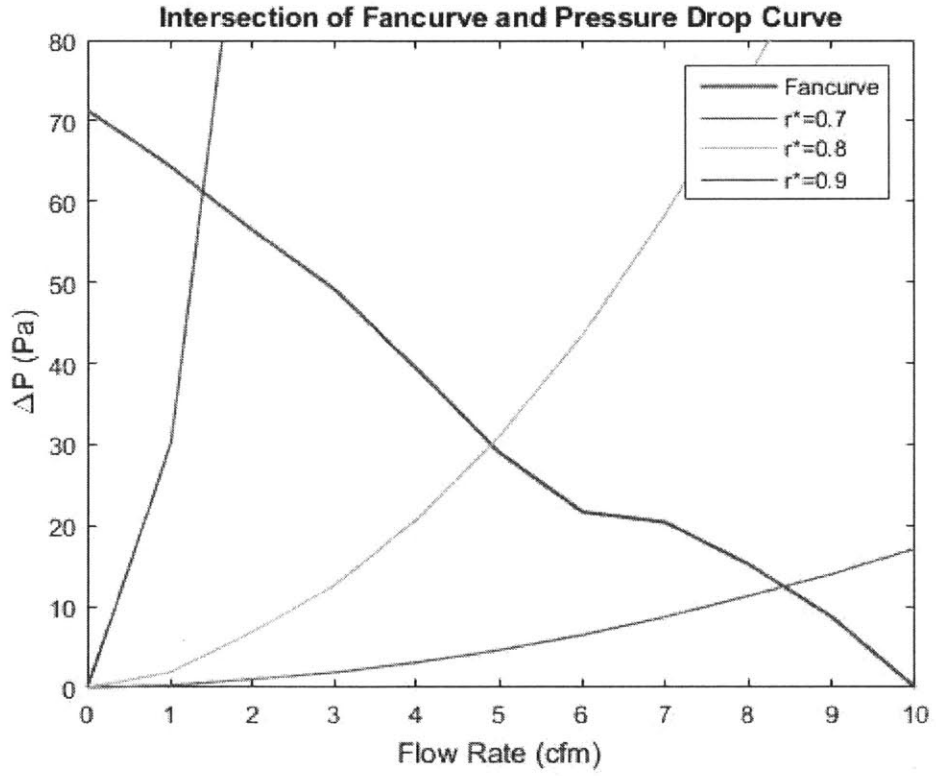

Fig 14: Graph showing the intersections of the fancurve (Obtained and reproduced from spec sheet. No smoothing was applied in order to preserve the correct shape and values) and the ΔP vs flow rate curves for a few values of r^*. The intersections of these graphs give the predicted flow rates for each annulus.

Now that we have the predicted flow rate, $\dot{V}$, given a particular r^*, we can determine that

Mass flow rate,

$$\dot{m} = \frac{\rho \dot{V}}{60} \quad (16)$$

And

$$Re_x = \frac{\dot{V}\left(\frac{r_{mot}}{r^*} - r_{mot}\right)}{30\vartheta\pi\left(\frac{r_{mot}^2}{r^{*2}} - r_{mot}^2\right)} \quad (17)$$

$$Pr_{air} = 0.7$$

As such, we can find an expression for h_{air} for laminar and turbulent flow

$$h_{air,lam} = \frac{0.332\sqrt[3]{0.7}k_{housing}}{x}\sqrt{\frac{\dot{V}\left(\frac{r_{mot}}{r^*} - r_{mot}\right)}{30\vartheta\pi\left(\frac{r_{mot}^2}{r^{*2}} - r_{mot}^2\right)}}^2 \quad (18)$$

$$h_{air,turb} = \frac{0.332\sqrt[3]{0.7}k_{housing}}{x}\sqrt{\left(\frac{\dot{V}\left(\frac{r_{mot}}{r^*} - r_{mot}\right)}{30\vartheta\pi\left(\frac{r_{mot}^2}{r^{*2}} - r_{mot}^2\right)}\right)^4}^5 \quad (19)$$

We can therefore find a bulk coefficient of thermal convection, $\bar{h}$, and resultantly find the bulk winding temperature, T_w as r^* changes. See Fig 15 below.

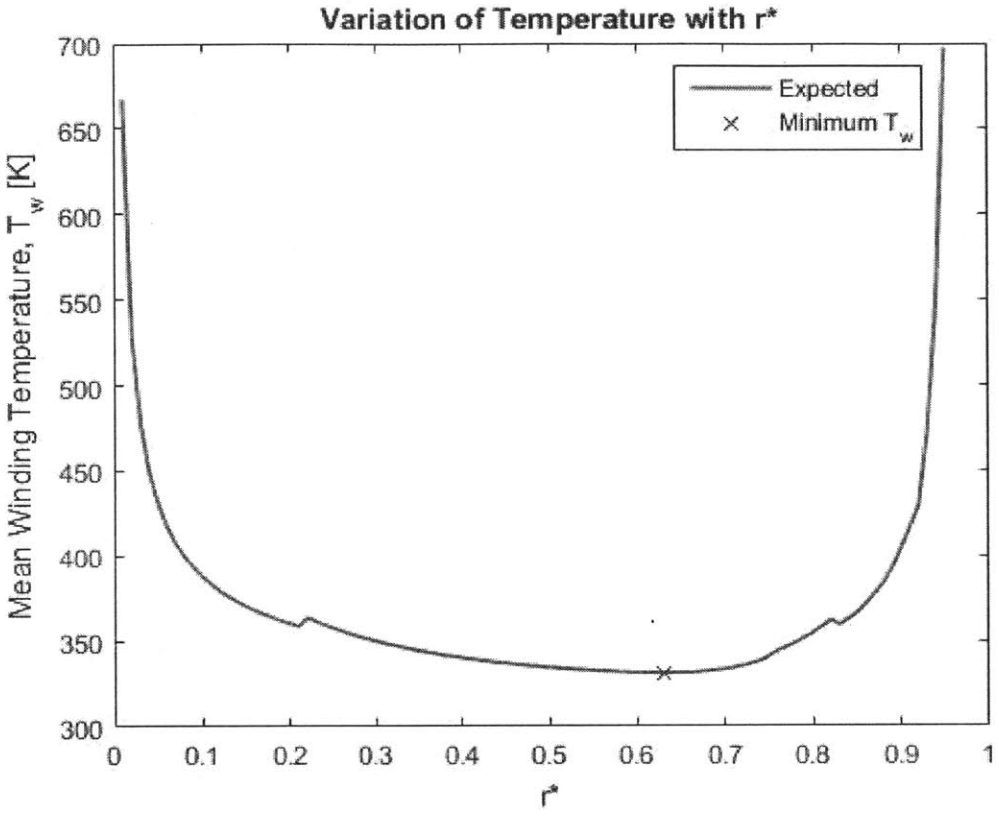

Fig 15: Graph of Temp vs $r^* = \frac{r_{mot}}{r_o}$. Demonstrates optimal choice at $r^* = 0.63$.

5.2 Experimental

The apparatus remains the same from the previous experiments. In this setup however, we add an annulus around the motor and a fan over the annulus.

5.2.1 Aims

Measure the new housing to ambient thermal resistance for each annulus.

Measure the steady state temperature in each case

Calculate the total mass added

Calculate the corresponding torque and specific torque.

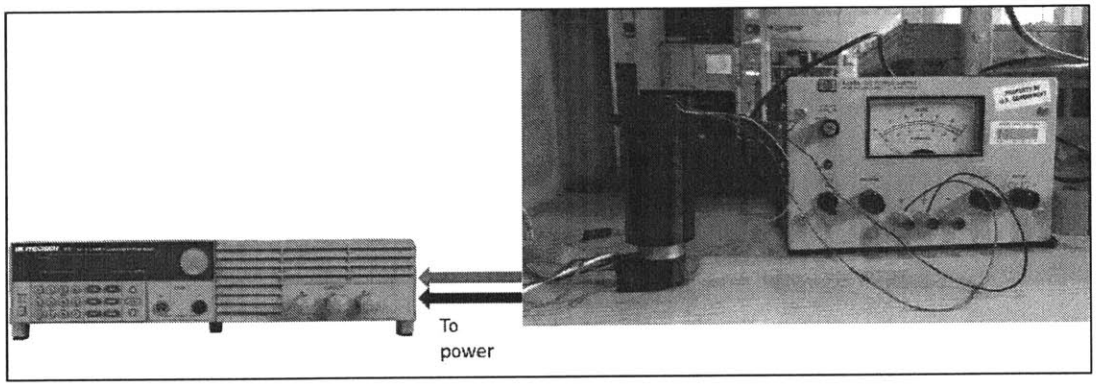

Fig. 16: Diagram showing how apparatus was set up.

5.2.2 Apparatus

1. Programmable power supply (used to power motor - see Appendix 1): 9152 30V/18A 540W, B&K Precision, Yorba Linda, CA, USA
2. DC brushless motor: EC-4 pole 48V, Maxon Motors, Sachseln, Switzerland (See Appendix 2)
3. Timer
4. Three 3D printed annuli of various sizes (40mm, 35mm, 31mm)

5. DC power supply (used to power fan – see Appendix 3): 6282A, Hewlett Packard, Palo Alto, CA, USA
6. Voltmeter/Ohmmeter (built into power source)
7. 10 cfm rated electronics fan: PSAD14010BH, Aavid Thermalloy, Laconia NH, USA (See Appendix 4)
8. Computer to control setup via MATLAB

5.2.3 Procedure

1. Set up the apparatus as shown in figure 16.
2. Note T_a and record it
3. Pick one of the three annuli and position the fan to push air over the motor.
4. Turn on the DC power supply to turn on the fan and position the fan in cross flow, 5mm away from the motor.
5. On the programmable power supply, set I to $5A$ and V to $2.5V$ to create a power output of 10W.
6. At each time step, sample I and V and calculate the corresponding R. Find the winding temperature and alter the input current and voltage to maintain the power input. Do this for one time constant.
7. Plot data and fit a curve to the data to predict the steady state winding resistance.
8. Use the steady state resistance to determine steady state T_w and the projected steady state τ.
9. Change the flow direction to pull air over the motor and repeat steps 5 to 8.
10. Using the other annuli, repeat steps 2 through 9.

5.3 Results

Air flow pushed along motor length:

	Ann. 1 ($r^* = \frac{30mm}{40mm} = 0.75$)	Ann. 2 ($r^* = \frac{30mm}{35mm} = 0.86$
Maximum Resistance, R [Ω]	0.4092	0.4127
Steady State Winding Temperature, T_w [K]	343.8	346.4
Steady State Torque, τ [Nm]	0.1296	0.1292
Augmented Mass, m [kg]	0.3299	0.3324
Torque Density, τ_{dens} [$Nmkg^{-1}$]	0.3928	0.3887
Corresponding R_{ha} [KW^{-1}]	4.38	4.65

Table 2: Table listing steady state resistance, temperature, torque, specific torque and the corresponding thermal resistance for each annulus under 'pushed' air flow.

Air flow pulled along motor length:

	Ann. 1 ($r^* = \frac{30mm}{40mm} = 0.75$)	Ann. 2 ($r^* = \frac{30mm}{35mm} = 0.86$
Maximum Resistance, R [Ω]	0.4133	0.4184
Steady State Winding Temperature, T_w [K]	346.8	350.6
Steady state Torque, τ [Nm]	0.1291	0.1285
Augmented Mass, m [kg]	0.3299	0.3324
Torque Density, τ_{dens} [$Nmkg^{-1}$]	0.3913	0.3866
Corresponding R_{ha} [KW^{-1}]	4.69	5.07

Table 3: Table listing steady state resistance, temperature, torque, specific torque and the corresponding thermal resistance for each annulus under 'pulled' air flow.

Figure 17 below shows how the experimental winding temperature values agree with the predictions based on the model.

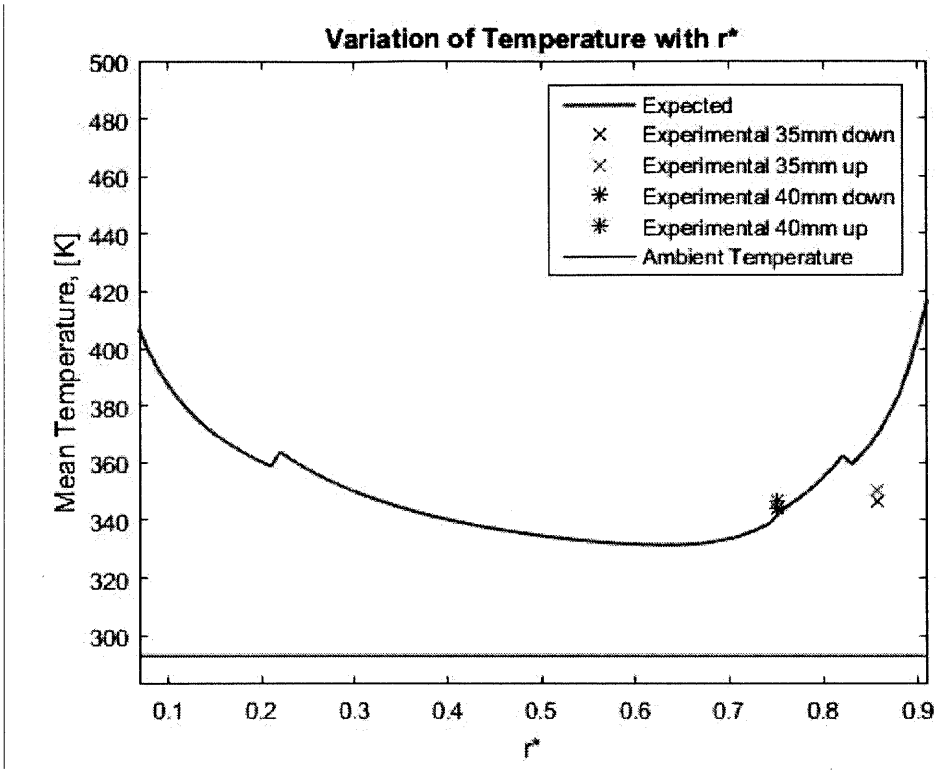

Fig. 17: Zoomed in view of Fig. 15

Chapter 6 - Discussion

Results show that the winding temperature has been reduced, but residual heat from remaining thermal resistance causes an operating temperature of approximately 340K. In relation to the ambient temperature of 296K, this operating temperature is improved from the unaltered motor steady state operating temperature of $413.17K$. For a power input of 10W, the winding temperature can be reduced by $73K$ with the use of a simple fan. This corresponds to a maximum decrease in R_{ha} of approximately 68%.

It is worth noting, however, that the actual value obtained for R_{ha} ($11.5KW^{-1}$) without any augmentation exceeds the specified value of $7.4KW^{-1}$ by $4KW^{-1}$. A possible explanation may be afforded by considering information presented by Maxon. According to key information presented on Maxon motors[5], "thermal resistance R_{th1}" (which is R_{wh} in our case) "describes the heat transfer between the motor winding and the stator (magnetic return and magnet), whereas R_{th2}" (corresponding to R_{ha} in our case) "describes the heat transfer from the housing to the environment... The values specified in the data sheets for thermal resistances and the maximum continuous current were determined in a series of tests, in which the motor was end-mounted onto a vertical plastic plate. The modified thermal resistance R_{th2} that occurs in a particular application must be determined using original installation and ambient conditions." In this thesis the original conditions have not necessarily been replicated. In addition, R_{th1} (our R_{wh}) describes winding to stator thermal resistance, not necessarily winding to housing thermal resistance. As such, we may be capturing the stator to housing thermal resistance in the observed discrepancy. This discrepancy may surface as errors in other results. It is also a possibility that the discrepancy may be attributed to the stall torque condition of the motor during experiments. Dynamic conditions may provide a more accurate prediction of the housing to ambient thermal resistance.

One further significant source of error may exist in the fact that the motor was given a steady power input of $10W$ with a current of approximately $5A$. This amperage exceeds the maximum allowable continuous current as stipulated by the data sheet, but unfortunately could not be changed. However, a current of 5A

corresponds to a projected torque of $0.138\ Nm$ which is within the torque limit. It is possible then that $5A$ places the experiments in a buffer region that protects the windings. However, the windings were measured to be at a maximum of $413.17K$ during unfanned operation. This sits comfortably in the 403.15K – 423.15K range over which the laminate begins to degenerate. Hence, it is possible that at 5A, we started to damage the laminate of the windings.

The above sources of error were thought to be the most significant. Other more negligible sources of error lie in the assumptions that were made to simplify modeling. The entrance region was found to be small compared to the full length of the motor (<8%). As such the entrance region was ignored in modeling. A parallel flat plate model approximation was also used. This was done under the assumption that it was equivalent enough to the motor-annulus configuration for differences to be minimal. One other assumption stipulated that bulk values were sufficient. A bulk value for h was used and gave a bulk value for T_h. That is to say that we assumed that these values were uniform over the entire motor. In reality, these values change locally over the motor. These values also vary in time whereas the model ignored transient effects. Other assumptions made were that there was no loss in flow velocity between the beginning and end of the annulus, that imperfections on the inner surface of the annuli did not disrupt flow and that the motor windings were made of pure copper. These assumptions all simplified modeling and were thought to not too significantly affect the integrity of results and analysis. However, they will need to be explored to determine their true impact on the model.

One particular assumption that needs to be addressed with this model is that transitions between laminar and turbulent flow would minimally affect the resultant winding temperature and are negligible. It was anticipated that there would be one discontinuity in figure 16 where the flow switched between turbulent and laminar and it was expected that this discontinuity would not be too jarring. However, from the graph, the distinction is noticeable. Further to this, the discontinuity appears in two places, suggesting that smoothly changing annular size does not necessarily imply straightforward transition between flow types

as annular size changes. From modeling calculations, as r^* increases the annuli appear to create parameters that give Reynolds numbers which suggest a transition from laminar flow, to turbulent flow and back to laminar flow. See figure 18 below.

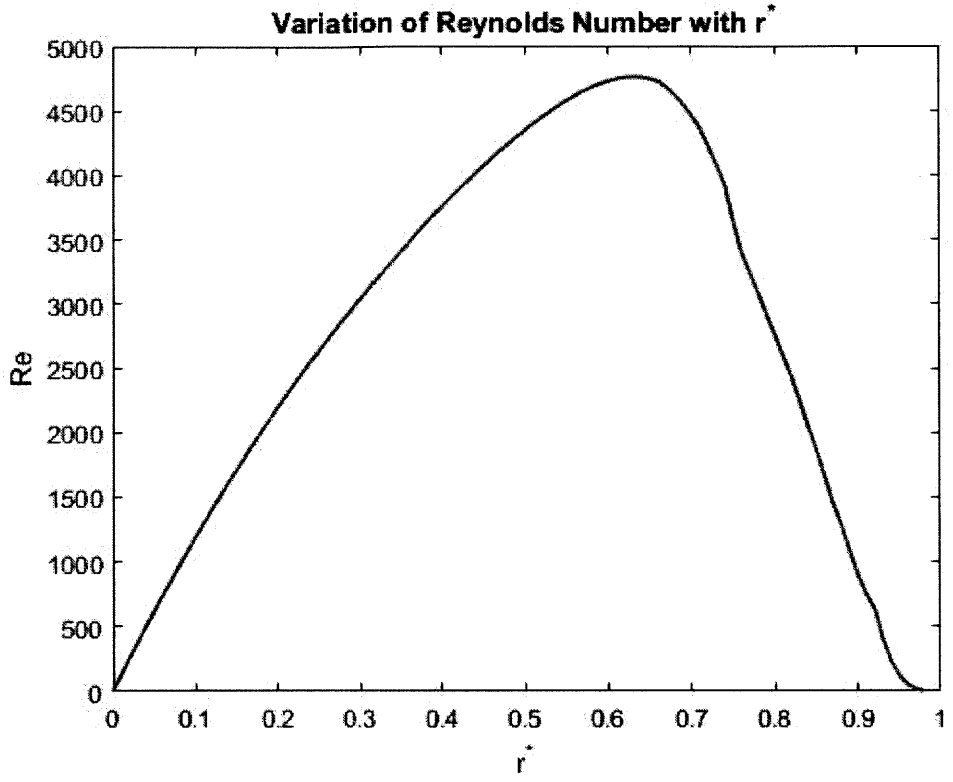

Fig. 18: Graph demonstrating relationship between r^* and Re.

This is a smooth transition, but the correlations in equations (18) and (19), which separately govern laminar and turbulent flow, do not represent this switching back and forth well. They behave as piecewise functions rather than continuous ones and therefore give rise to the two discontinuities observed in figures 17 and 15. Future work can include a close inspection of these discontinuities to explain the apparent phenomenon. Other changes that should be made to the approach to this thesis are testing using more than three annuli, ensuring to include $r^* = 0.63$, as well as using a larger range of annular sizes in experiments.

If we now compare the model and the results, we can see that the results are centered around the model. There aren't enough points to definitively verify the model, but the close agreement between the prediction and actual values is promising. Looking at the experimental data in relation to the graph, the points seem to lie on a curve with a smaller change in gradient. This suggests that the actual graph of T_w vs r^* is flatter than the model suggests.

As such, using an annulus may not necessarily the best overall solution.

The expected torque density of the different setups varied from $0.383 Nmkg^{-1}$ to $0.393 Nmkg^{-1}$. This is a range of only $0.010 Nmkg^{-1}$ This small range suggests that with the annuli used in this investigation, there is no appreciable improvement in performance. A more extensive investigation is, however, necessary to fully validate this trend.

Further to this, even simpler methods can be more effective. For example, according to a datasheet on key information for Maxon motors[5], motors with metal flanges can have R_{ha} decreased by up to 80% whereas with the best annulus of $r^* = 0.63$, R_{ha} can be decreased by 68%. As such, it appears that simply adding a metal flange may yield even better results. However, it is difficult to say definitively as one would have to consider the torque-mass ratio the flange provides. This is dependent on the flange geometry. It is therefore evident that there do exist methods of improving motor performance for robotic prosthesis and exoskeleton applications that are simpler and competitive with the annulus approach. However, further work needs to be carried out to determine the best method.

Chapter 7 - Conclusion

It has been demonstrated that for a given motor and current input, adding a fan and/or an annulus does not appreciably improve motor performance, though it does decrease housing to ambient thermal resistance significantly (an improvement of 68% was shown via the experiments outlined here). Better results may be obtained using the optimal annular size of $r^* = 0.63$ (89% decrease in R_{ha} and an improved torque density of $0.414 Nmkg^{-1}$ is projected in comparison to a density of 0.393 for an unaltered motor). However, these improvements are not striking suggesting that an approach using annuli and a fan is not the most appropriate choice. Nevertheless, this thesis does show that simple augmentation of the DC brushless motors used in biomechatronic applications has the potential to alter their torque density. By extension the performance of the devices in which they are used can also be improved.

Further work is necessary though in order to more explicitly establish the pros and cons of such augmentation. For the approach taken in this thesis, more detailed modeling is necessary in order to fully validate or invalidate its merits. Equations that more closely model brushless motor operation are necessary. Full commutation should also be implemented in order to verify the projected torques given in the results. In addition, work needs to be done to determine the best fan (only Aavid Thermalloy's PSAD14010BH model was considered) and the entrance region of flow should be factored in to the mathematical model. Limitations such as how one would mount the annulus and fan on to a prosthesis or exoskeleton would also need to be addressed. Subsequently, other methods should be investigated against which the annulus-fan approach can be weighed. This requires some innovation in order to prove and disprove other potential methods of motor augmentation.

Modifying the DC brushless motors currently used in biomechatronic applications in order to increase their capabilities definitely holds promise. This thesis suggests as such. It is hoped that the work presented here adds to the growing wealth of knowledge and research in the field of biomechatronics.

Chapter 8 - Appendix

8.1 Appendix 1 - Specification Sheet for B&K Motor Power Supply: Mod. # 9152

Models 9150, 9151, 9152, 9153

Parameter		9150	9151	9152	9153
Output Ratings (0 °C - 40 °C)	Voltage	0 - 5.2 V	0 - 20 V	0 - 30 V	0 - 60 V
	Current	0 - 60 A	0 - 27 A	0 - 18 A	0 - 9 A
	LVP*	0 - 5.5 V	0 - 21 V	0 - 31 V	0 - 61 V

Load Regulation ±(%of output+offset)	Voltage	<0.01% + 2 mV	<0.01% + 1 mV	<0.01% + 1 mV
	Current	<0.1% + 10 mA	<0.1% + 5 mA	<0.1% + 2 mA
Line Regulation ±(%of output+offset)	Voltage	<0.02% + 0.1 mV	<0.02% + 1 mV	<0.02% + 1 mV
	Current	<0.1% + 1 mA	<0.01% + 1 mA	<0.01% + 0.1 mA
Programming resolution	Voltage	0.1 mV	1 mV	1 mV
	Current	1 mA	1 mA	0.1 mA
Readback/Meter resolution	Voltage	0.1 mV	0.1 mV	0.1 mV
	Current	1 mA	0.1 mA	0.1 mA
Front Panel setting resolution	Voltage	0.1 mV	0.5 mV	0.5 mV
	Current	1 mA	1 mA	1 mA
Programming accuracy, 12 months (25 °C ± 5 °C) ±(%of output+offset)	Voltage	<0.02%+2 mV	<0.02%+6 mV	<0.02%+12 mV
	Current	<0.1%+30 mA	<0.1%+15 mA	<0.05%+10 mA
Readback / Meter accuracy 12months (25 °C ± 5 °C) ±(%of output+offset)	Voltage	<0.02%+1.5 mV	<0.02%+3 mV	<0.02%+6 mV
	Current	<0.05%+15 mA	<0.05%+10 mA	<0.05%+5 mA
Ripple & Noise (20 Hz ~20 MHz)	Voltage	≤0.005%+3 mVp-p	≤0.005%+3 mVp-p	≤0.005%+4 mVp-p
	Current	15 mArms	5 mArms	3 mArms
Temperature coefficient, (0 °C~40 °C) ±(%of output+offset)	Voltage	<0.02%+2 mV	<0.02%+5 mV	<0.02%+10 mV
	Current	<0.1%+30 mA	<0.1%+15 mA	<0.05%+5 mA
Readback temperature, coefficient, ±(%of output+offset)	Voltage	<0.02%+2 mV	<0.02%+5 mV	<0.02%+10 mV
	Current	<0.1%+20 mA	≤0.05%+10 mA	≤0.05%+5 mA
DVM Accuracy	Voltage	0~12 V range: 0.02%+2 mV 0~40 V range: 0.02%+3 mV		
DVM Resolution	Voltage	0~12 V range: 0.1 mV 0~40 V range: 1 mV		
Ohm meter	mΩ	Accuracy: 0.1%, for Voltage and Current >= 10% of FS (full scale) Accuracy: 0.3% for Voltage and Current = 3 to 10% of FS		
Weight	net	63.9 lbs (29 kg)		
Dimensions	WxHxD	429 mm × 88.2 mm × 458.9 mm 16.88(W) x 3.47(H) x 18.06(D) inch		

*) LVP: Limit Voltage Protection. Limits the voltage than can be set either via the front panel or remote control command.

NOTE: Specifications and information are subject to change without notice. Please visit www.bkprecision.com for the most current product information.

8.2 Appendix 2 - Specification Sheet for Motor Used: Mod. # 305015.

EC-4pole 30 Ø30 mm, brushless, 200 Watt

High Power

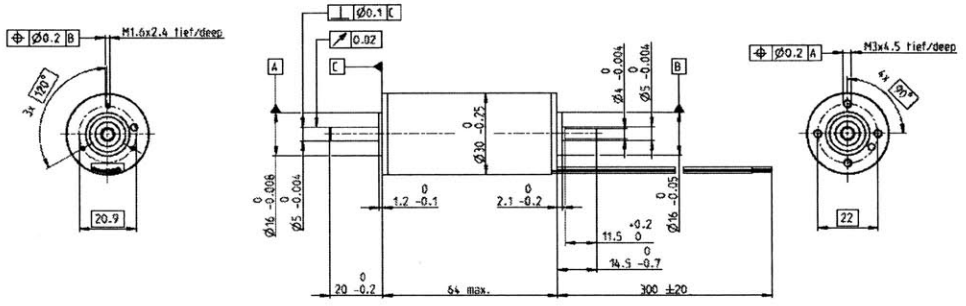

M 1:2

Stock program
Standard program
Special program (on request)

Part Numbers	305013	305014	305015
Motor Data			
Values at nominal voltage			
1 Nominal voltage V	24	36	48
2 No load speed rpm	16700	16700	16500
3 No load current mA	728	485	356
4 Nominal speed rpm	16100	16200	16000
5 Nominal torque (max. continuous torque) mNm	94.6	94.2	92.9
6 Nominal current (max. continuous current) A	7.58	5.03	3.68
7 Stall torque mNm	3220	3510	3430
8 Stall current A	236	171	124
9 Max. efficiency %	89.4	89.9	89.8
Characteristics			
10 Terminal resistance phase to phase Ω	0.102	0.21	0.386
11 Terminal inductance phase to phase mH	0.0163	0.0368	0.0653
12 Torque constant mNm/A	13.6	20.5	27.6
13 Speed constant rpm/V	700	466	346
14 Speed/torque gradient rpm/mNm	5.21	4.78	4.83
15 Mechanical time constant ms	1.82	1.67	1.69
16 Rotor inertia gcm²	33.3	33.3	33.3

Specifications

Thermal data
17 Thermal resistance housing-ambient 7.4 K/W
18 Thermal resistance winding-housing 0.21 K/W
19 Thermal time constant winding 2.11 s
20 Thermal time constant motor 1180 s
21 Ambient temperature -20...+100°C
22 Max. winding temperature +155°C

Mechanical data (preloaded ball bearings)
23 Max. speed 25000 rpm
24 Axial play at axial load < 8.0 N 0 mm
> 8.0 N 0.14 mm
25 Radial play preloaded
26 Max. axial load (dynamic) 5.5 N
27 Max. force for press fits (static) 73 N
(static, shaft supported) 1300 N
28 Max. radial load, 5 mm from flange 25 N

Other specifications
29 Number of pole pairs 2
30 Number of phases 3
31 Weight of motor 300 g

Values listed in the table are nominal.

Connection motor (Cable AWG 18)
black Motor winding 2
white Motor winding 3
red Motor winding 1
Connection sensors (Cable AWG 26)
black/grey Hall sensor 2
blue GND
green V_{Hall} 3...24 VDC
red/grey Hall sensor 1
white/grey Hall sensor 3
Wiring diagram for Hall sensors see p. 33

Operating Range Comments

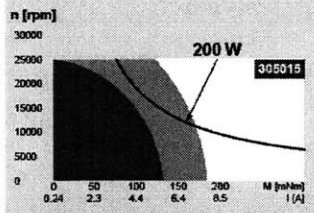

Continuous operation
Continuous operation with reduced thermal resistance Rth_2 50%
Intermittent operation
Assigned power rating

maxon Modular System Overview on page 20–25

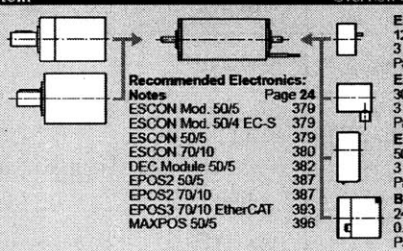

Planetary Gearhead
Ø32 mm
8 Nm
Page 310
Planetary Gearhead
Ø42 mm
3 - 15 Nm
Page 315

Recommended Electronics:

Notes	Page 24
ESCON Mod. 50/5	379
ESCON Mod. 50/4 EC-S	379
ESCON 50/5	379
ESCON 70/10	380
DEC Module 50/5	382
EPOS2 50/5	387
EPOS2 70/10	387
EPOS3 70/10 EtherCAT	393
MAXPOS 50/5	396

Encoder MR
128 - 1000 CPT,
3 channels
Page 355
Encoder 2RMHF
3000 - 5000 CPT,
3 channels
Page 360
Encoder HEDL 5540
500 CPT,
3 channels
Page 367
Brake AB 20
24 VDC
0.1 Nm
Page 406

8.3 Appendix 3 - Specification Sheet for HP 6286A DC Power Supply

Table 1-1. Specifications

INPUT:
105-125 VAC, single phase, 50-60Hz, 5.5A, 320W.

OUTPUT:
0-20 volts @ 0-10 amps.

LOAD REGULATION:
Constant Voltage -- Less than 0.01% plus 1mV for a full load to no load change in output current.
Constant Current -- Less than 0.05% plus 1mA for a zero to maximum change in output voltage.

LINE REGULATION:
Constant Voltage -- Less than 0.01% plus 1mV for any line voltage change within the input rating.
Constant Current -- Less than 0.05% plus 1mA for any line voltage change within the input rating.

RIPPLE AND NOISE:
Constant Voltage -- Less than 500μV rms.
Constant Current -- Less than 5mA rms.

OPERATING TEMPERATURE RANGES:
Operating: 0 to 50°C. Storage: -20 to +85°C.

TEMPERATURE COEFFICIENT:
Constant Voltage -- Less than 0.02% plus 500μV per degree Centigrade.
Constant Current -- Less than 0.02% plus 5mA per degree Centigrade.

STABILITY:
Constant Voltage -- Less than 0.10% plus 2.5mV total drift for 8 hours after an initial warm-up time of 30 minutes at constant ambient, constant line voltage, and constant load.
Constant Current -- Less than 0.10% plus 25mA total drift for 8 hours after an initial warm-up time of 30 minutes at constant ambient, constant line voltage, and constant load.

INTERNAL IMPEDANCE AS A CONSTANT VOLTAGE SOURCE:
Less than 0.001 ohm from DC to 100Hz.
Less than 0.01 ohm from 100Hz to 1kHz.
Less than 0.2 ohm from 1kHz to 100kHz.
Less than 2.0 ohms from 100 kHz to 1 MHz.

TRANSIENT RECOVERY TIME:
Less than 50μsec for output recovery to within 15 mv following a current change in the output equal to the current rating of the supply or 5 amperes, whichever is smaller.

OVERLOAD PROTECTION:
A continuously acting constant current circuit protects the power supply for all overloads including a direct short placed across the terminals in constant voltage operation. The constant voltage circuit limits the output voltage in the constant current mode of operation.

METER:
The front panel meter can be used as either a 0-24 or 0-2.4 volt voltmeter or as a 0-12 or 0-1.2 amp ammeter.

OUTPUT CONTROLS:
Coarse and fine voltage controls and coarse and fine current controls provide continuous adjustment over the entire output span.

OUTPUT TERMINALS:
Three "five-way" output posts are provided on the front panel and an output terminal strip is located on the rear of the chassis. All power supply output terminals are isolated from the chassis and either the positive or negative terminal may be connected to the chassis through a separate ground terminal. If the front panel terminals are used, the load regulation will be 0.5mV per ampere greater, due to the front terminal resistance.

ERROR SENSING:
Error sensing is normally accomplished at the front terminals if the load is attached to the front or at the rear terminals if the load is attached to the rear terminals. Also, provision is included on the rear terminal strip for remote sensing.

REMOTE PROGRAMMING:
Remote programming of the supply output at approximately 200 ohms per volt in constant voltage is made available at the rear terminals. In constant current mode of operation, the current can be remotely programmed at approximately 100 ohms per ampere.

COOLING:
Convection cooling is employed. The supply has no moving parts.

SIZE:
5¼" H x 16" D x 8½" W. Two of the units can be mounted side by side in a standard 19" relay rack.

WEIGHT:
30 lbs. net. 40 lbs. shipping.

FINISH:
Light gray front panel with dark gray case.

POWER CORD:
A three-wire, five-foot power cord is provided with each unit.

8.4 Appendix 4 - Specification Sheet for Fan Used: Mod. # PSAD14010BH

AAVID THERMALLOY

Superior Series (PS)
40mm x 40mm x 10mm

- » Bearing Type: FLB, Ball Bearing
- » Function Type (Optional) : FG Signal, RD Signal, PWM
- » Protection:
  - Auto Restart Protection
  - Polarity Reverse Protection
- » Lead Wire:
  - UL 1061 AWG #28 or Equivalent
  - Red Wire: Positive (+)
  - Black Wire: Negative (-)
  - Yellow Wire: FG Signal
  - White Wire: RD Signal
  - Blue Wire: PWM

DIMENSIONS DRAWING

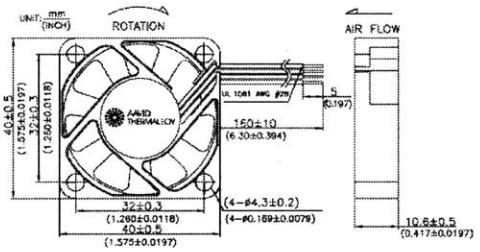

PERFORMANCE CURVES

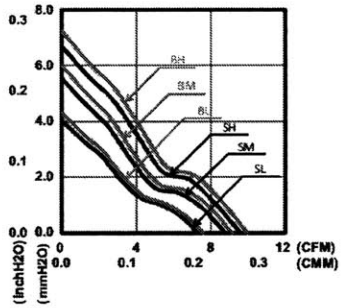

SPECIFICATION

Model	Function Type	Rated Voltage	Operating Voltage	Rated Current	Input Current	Input Power	Rated Speed	Air Flow		Air Pressure		Noise
		VDC	VDC	Amp	Amp	Watt	RPM	CMM	CFM	mmH2O	InH2O	dBA
PSAD04010SL	P000/PF00 M000/MF00	5	4~5.75	0.12	0.08	0.40	6200	0.21	7.36	4.03	0.16	29.0
PSAD04010SM		5	4~5.75	0.18	0.13	0.65	7200	0.25	8.78	5.53	0.22	32.5
PSAD04010SH		5	4~5.75	0.24	0.18	0.90	7900	0.27	9.60	6.68	0.26	35.5
PSAD14010SL	P000/PF00 M000/MF00	12	6~13.8	0.07	0.06	0.66	6200	0.21	7.36	4.03	0.16	29.0
PSAD14010SM		12	6~13.8	0.09	0.07	0.84	7200	0.25	8.78	5.53	0.22	32.5
PSAD14010SH		12	6~13.8	0.13	0.10	1.20	7900	0.27	9.60	6.68	0.26	35.5
PSAD04010BL	P000/PF00 M000/MF00	5	4~5.75	0.12	0.08	0.40	6400	0.22	7.60	4.29	0.17	28.5
PSAD04010BM		5	4~5.75	0.18	0.13	0.65	7500	0.26	9.15	6.00	0.24	33.0
PSAD04010BH		5	4~5.75	0.24	0.16	0.80	8300	0.28	10.00	7.24	0.29	35.5
PSAD14010BL	P000/PF00 M000/MF00	12	6~13.8	0.07	0.06	0.66	6400	0.22	7.60	4.29	0.17	28.5
PSAD14010BM		12	6~13.8	0.09	0.07	0.84	7500	0.26	9.15	6.00	0.24	33.0
PSAD14010BH		12	6~13.8	0.13	0.10	1.20	8300	0.28	10.00	7.24	0.29	35.5

* Specifications are subject to change without notice

Chapter 9 - Bibliography

[1] LeMoyne, R., "Advances for Prosthetic Technology: From Historical Perspective to Current Status to Future Application", 2016, Springer Japan, p. 80, 5 May 2016. http://link.springer.com/book/10.1007%2F978-4-431-55816-3

[2] Moreno, J. C., Turowska, E., Pons, J. L., Ferris, D. P., De Roy, K., Yamamoto, K., Bastos-Filho, T. F., Sarcinelli-Filho, M., Ferreira, A., Celeste, W. C., Silva, R. L., Martins, V. R., Cavalieri, D. C., Filgueira, P. N. S. and Arantes, I. B. (2008) Wearable Lower Limb and Full-Body Robots, in Wearable Robots: Biomechatronic Exoskeletons (ed J. L. Pons), John Wiley & Sons, Ltd, Chichester, UK. doi: 10.1002/9780470987667.ch9

[3] Maxon Academy, "maxon DC motor; Permanent magnet DC motor with coreless winding", ©2012, maxon motor ag, www.maxonmotor.com, 27 April 2016, http://www.maxonmotorusa.com/medias/sys_master/root/8803450617886/maxonDCmotor-Notes.pdf?attachment=true

[4] Montone, D., "Temperature Effects on Motor Performance", 5 May 2016. http://www.pittman-motors.com/Portals/0/Resources/Temperature_Effects_On_DC_Motor_Performance.pdf

[5]maxon motor. "maxon DC motor and maxon EC motor Key Information", 2014, 27 April 2016. http://www.maxonmotor.com/medias/sys_master/root/8815460712478/DC-EC-Key-Information-14-EN-42-50.pdf?attachment=true

[6] Kuphaldt, T.R., "Lessons in Electric Circuits; Vol. 1 – Direct Current (DC); Chapter 12 – Physics of Conductors and Insulators", 1996-Present, 28 April 2016, http://www.allaboutcircuits.com/textbook/direct-current/chpt-12/temperature-coefficient-resistance/

[7] Song, Y., Zhu, D., "High Density Data Storage - Principle, Technology, and Materials - 1.2.4.2 Curie-Weiss Law", 2009, World Scientific, 25 April 2016, http://app.knovel.com/hotlink/pdf/id:kt008J2534/high-density-data-storage/curie-weiss-law

[8]Woollenweber, William E., and Edward M. Halimi. "Motor-driven centrifugal air compressor with internal cooling airflow." U.S. Patent 6,102,672, issued August 15, 2000, October 2015

[9] Bergman, T.L., Lavine, A.S., Incropera, F.P., DeWitt, D.P., "Fundamentals of Heat and Mass Transfer 7th Edition", 2011, Wiley Hoboken, NJ, p 441, October 2016 –May 2016.

[10] Bergman, T.L., Lavine, A.S., Incropera, F.P., DeWitt, D.P., "Fundamentals of Heat and Mass Transfer 7th Edition", 2011, Wiley Hoboken, NJ, p 443, October 2016 –May 2016.

[11] Kays, W. M., London, A. L., "Compact Heat Exchangers – Third Edition", 1984, McGraw Hill U.S.A., October 2015 – May 2016.

[12] Schwarz, D. M., "intersections.m", ©2008, Mathworks Forum (www.mathworks.com), November 2016.